



Published in final edited form as:

J Nucl Med. 2011 July ; 52(7): 1068–1072. doi:10.2967/jnumed.110.085944.

Lymphatic drainage mapping of prostate using filtered ^{99m}Tc-sulfur nanocolloid and SPECT/CT

Youngho Seo^{1,2,3}, Carina Mari Aparici^{1,4}, Chien Peter Chen², Charles Hsu², Norbert Kased², Carole Schreck¹, Nick Costouros¹, Randall Hawkins^{1,3}, Katsuto Shinohara^{2,5}, and Mack Roach III^{2,5}

¹ Department of Radiology and Biomedical Imaging, University of California, San Francisco, California

² Department of Radiation Oncology, Helen Diller Family Comprehensive Center, University of California, San Francisco, California

³ Joint Graduate Group in Bioengineering, University of California, San Francisco and Berkeley, California

⁴ San Francisco Veterans Affairs Medical Center, San Francisco, California

⁵ Department of Urology, University of California, San Francisco, California

Abstract

We have developed a practice procedure of prostate lymphoscintigraphy using SPECT/CT and filtered ^{99m}Tc-sulfur nanocolloid.

Methods—A total of 10 patients were enrolled for this study, and all administered with the radiotracer prepared using a 100-nm membrane filter at a commercial radiopharmacy. Whole-body scans and SPECT/CT studies were performed within 1.5–3 hours after the radiotracer administration directly into six locations of the prostate gland under a transrectal ultrasound guide. Radiation dose was estimated from the first 3 patients. The lymphatic drainage mapping and identification of lymph nodes were performed.

Results—Radiation dose estimates of filtered ^{99m}Tc-sulfur nanocolloid from the first three patients were in the range of 3.9–5.2 mSv/MBq. Our results showed the locations of lymph nodes drained from the prostate gland are similar to those found using ^{99m}Tc-Nanocoll.

Conclusion—Without the proprietary radiolabeled nanocolloid indicated for lymphoscintigraphy, prostate lymph node mapping and identification were feasible using filtered ^{99m}Tc-sulfur nanocolloid.

Keywords

prostate cancer; sulfur colloid; SPECT/CT; lymphatic mapping; sentinel node

INTRODUCTION

It is estimated that 50% or more patients of high risk prostate cancer will relapse after definitive treatment (1). There are substantial data suggesting many of these relapses may be

due to microscopic metastasis in pelvic lymph nodes (2–4). Recent surgical data indicated that the incidence of positive nodes is higher than once thought (2).

Nomogram predictors (5) help identify potential high risk of involved pelvic nodes. In order to confirm the microscopically involved nodes, lymphadenectomy combined with a pathologic analysis is necessary. Radical prostatectomy combined with an extended pelvic lymph node dissection (6) is one of the standard treatments for localized prostate cancer. However, in some cases, this represents an overly aggressive and invasive approach.

External beam radiotherapy or brachytherapy is presented with the same challenges. However, there is no method to assess nodal involvements unless anatomical imaging shows enlarged (over 1 cm diameter) lymph nodes. There are recent studies that suggest therapeutic value to treating potentially involved nodes by radiation (1). For example, the phase III trial by the Radiation Therapy Oncology Group (RTOG-9413) demonstrated that prophylactic pelvic lymph node irradiation improves progression-free survival for high-risk patients, suggesting that treatment of the primary tumor and local lymph nodes can be curative (7).

Pelvic irradiation can increase the probability of treatment side effects. The exact volume of nodes to include in the radiation field is, therefore, critical, and has been much debated (8). Currently, most whole-pelvic radiotherapy planning is based on assumptions about standardized anatomic lymphatic drainage patterns (9). However, as shown in radioguided surgical lymph node dissection results, the patterns of each patient's lymphatic drainage of the prostate are highly variable (9,10).

Whole-pelvic irradiation of patient-specific lymphatic drainage with a highly conformal radiotherapy technique such as intensity-modulated radiotherapy (IMRT) could improve long-term tumor control outcomes (11). ^{99m}Tc -nanocolloids (colloidal particles smaller than 100 nm) can be used to achieve the goal of personalized whole-pelvic radiation planning (9,12).

The most popular ^{99m}Tc -nanocolloid is a commercial product called ^{99m}Tc -Nanocoll (GE Healthcare, Chalfont St. Giles, UK) that is colloid of human serum albumin (13). Extensive studies using this nanocolloid were performed to map sentinel lymph nodes of prostate (14–16). However, this product has not received the US Food and Drug Administration (FDA) clearance yet. In the United States, ^{99m}Tc -sulfur colloid is used in breast lymphoscintigraphy as well as for other applications (17). The ^{99m}Tc -sulfur colloid can be formed into nanocolloid by filtering using a 100-nm polycarbonate membrane filter, resulting in the particle size range similar to that of Nanocoll (13). The important factor that contributes to the kinetic properties of a radiocolloid is the distribution of particle size, which is yet to be studied for filtered ^{99m}Tc -sulfur nanocolloid for prostate lymphoscintigraphy.

We report our experiences from a feasibility study of developing a practice procedure of prostate lymphoscintigraphy using filtered ^{99m}Tc -sulfur nanocolloid and single photon emission computed tomography combined with CT (SPECT/CT).

MATERIALS AND METHODS

Human subject recruitment and adverse events monitoring

Subjects were recruited following a protocol approved by Institutional Review Board (IRB). The filtered ^{99m}Tc -sulfur nanocolloid, as an FDA-approved agent, was used for an open-label indication. The basic inclusion criteria include diagnosis of definitive prostate cancer,

and clinically eligible and scheduled for definitive IMRT with pelvic lymph nodal irradiation. Ten patients (ages 56–81 years and prostate-specific antigen levels 3.55–70 ng/mL) were enrolled. Reportable adverse events were communicated one week after the radiotracer administration. There was no reported adverse event related to the study.

Administration of filtered ^{99m}Tc -sulfur nanocolloid

There was an arrangement made with a local commercial radiopharmacy (GE Healthcare, Palo Alto, CA) that all orders for this study were to use the 100-nm membrane filter. Once the ^{99m}Tc -sulfur colloid is filtered through the 100-nm polycarbonate membrane filter, most colloidal particles (approximately 90%) are between 30 and 80 nm, with a peak at 53.9 nm (18). The administrations were performed in the Urology Clinic at the University of California, San Francisco (UCSF) Medical Center by one urologist (K.S.) using a transrectal ultrasound (TRUS) guide.

40.7–111 MBq of filtered ^{99m}Tc -sulfur nanocolloid were divided equally to 6 fractions of 0.5 ml volume, and were administered to 3 locations for each lobe (left and right) of the prostate gland. The sites of administrations were apex, mid portion, and base. Although the administrations were supposed to be evenly distributed to all six locations, we noted that there were uneven doses in some patients, resulting in uneven flow patterns of nodal uptake.

Whole-body and SPECT/CT imaging parameters

Our studies utilized a SPECT with low-mA CT scanner (Infinia Hawkeye 4, GE Healthcare) at the UCSF China Basin Imaging Center. All SPECT reconstructions were performed using an ordered subsets expectation maximization (OS-EM) algorithm involving CT-based attenuation correction. The SPECT projections were acquired with a 128×128 matrix over 60 angles covering 360° and 15 s per stop. The reconstructed images were 64×64×64 matrices post-filtered using a Butterworth filter. The whole-body scans with anterior-posterior views were performed before the SPECT/CT scans in order to ensure the sufficient spread of filtered ^{99m}Tc -sulfur nanocolloid out of the gland. The imaging time point of SPECT/CT covering pelvis and thorax, was between 1.5–3 hours postadministration. For the matching SPECT field of view, abdominal-pelvic CT was acquired without x-ray contrast agent. X-ray imaging parameters of 140 kVp tube voltage and 2.5 mA tube current were used, and the data were acquired using a 256×256 matrix and a 5 mm slice thickness. The filtered backprojection (FBP) algorithm provided by the manufacturer was used for CT reconstruction.

Radiation dose estimation using simple biokinetic data

For the first 3 patients, we performed whole-body scans after SPECT/CT, additional datasets for radiation dose estimates. For the logistical convenience, we applied a simple biokinetic analysis based on three time points of the distribution of the radiotracer. The first time point was not from imaging, but based on the assumption that initial radiotracer is localized only to the administration site, i.e., the prostate gland. The two additional time points were before and after SPECT/CT.

OLINDA|EXM software (version 1.1) (19) was used to estimate radiation dose. We calculated residence times in prostate, liver, and spleen from the whole-body scans using a conjugate-view method and phantom measurements that correct for image pixel difference of radioactivity in anterior and posterior views. For phantom measurements, we used a 6-ml syringe with a Lucite attenuator with a known activity calibrated using a dose calibrator.

Identification of lymph nodes and drainage mapping

The reading of the lymphoscintigraphy was performed by attending nuclear medicine physicians, and additionally re-reviewed by one of study investigators (C.M.A.). We used SPECT/CT images for identifying lymph nodes and drainage patterns. The identification of sentinel lymph nodes as well as all secondary nodes identifiable from the imaging studies was noted in the reports generated for the research examinations.

RESULTS

Radiation dose estimates

The reported radiation dose estimate for Nanocoll is 7.6 mSv/MBq effective dose (20). From the three patient data, we found that the effective dose of filtered ^{99m}Tc -sulfur nanocolloid, 3.9–5.2 mSv/MBq, was a little lower than that of Nanocoll (Table 1). Even with lower injected doses (40.7–111 MBq) that typical dose of Nanocoll (200 MBq), we were able to visualize lymph node uptakes drained from the injection site within 1.5–3 hours postadministration. From the radiation dose estimation data, we also found that the hepatic clearance of filtered ^{99m}Tc -sulfur nanocolloid is slightly faster than that of Nanocoll.

Lymph node identifications

One of our criteria for the success of this imaging procedure was to be able to image lymph node uptake outside of the prostate within 1–3 hours, and our results were consistent with the expectation.

Also as expected, lymph nodes were identified sometimes outside of pelvic area, a common feature of the prostatic lymphatic drainage pattern. Figures 1–3 show the patient demographic, injected dose, and lymphatic uptake locations reported for each patient. We also show a coronal view of SPECT/CT that displays at least one lymph node with uptake of filtered ^{99m}Tc -sulfur nanocolloid. Descriptive list of identified lymph nodes in the drainage of the prostate gland is also included in Figures 1–3.

DISCUSSION

In this report, we have shown that using nonproprietary filtered ^{99m}Tc -sulfur nanocolloid, prostate lymphoscintigraphy can be performed within 1.5–3 hours postinjection. The preparation of the radiotracer is important because the required size of colloid less than 100 nm is critical to ensure fast draining from the prostate gland as shown for a proprietary nanocolloid (Nanocoll). We recommend other users who will utilize our practice procedure to work with their respective local radiopharmacy to achieve prefiltering of sulfur colloid using a 100-nm membrane filter.

A limitation of our study was that only patients with an intact and previously untreated prostate were included. We chose not to include postprostatectomy patients because of uncertainty as to the appropriate places to inject the radiotracer in this setting and the known altered drainage patterns following previous therapies (15). Another limitation of our study is the absence of definitive proof as to exactly how this information may have altered our treatment fields. Such a detailed analysis is underway. Based on the work of others we do expect to find evidence supporting the routine use of sentinel node imaging (9,16).

Unlike common use of lymphoscintigraphy for surgical management of cancer, our prostate lymphoscintigraphy was to provide tomographic information of lymphatic drainage with sentinel and secondary nodes using SPECT/CT, so that radiation treatment planning for these patients can be performed using individualized irradiation fields. It was clear to us that

in at least two cases we substantially altered fields resulted from the sentinel node images. In these two cases, the primary drainage included common iliac nodes above the level of L5-S1 (our standard superior border). In addition, in all cases we applied slightly wider margins and delivered a slightly higher dose to sentinel nodal areas. We also used tighter margins and consequently lower doses to nonsentinel nodal drainage areas. This strategy, at least in theory, should result in enhanced nodal control and reduced toxicity due to smaller irradiated volumes to uninvolved normal tissues, such as the small bowel.

Finally, another interesting methodological approach that could enhance our practice procedure of SPECT/CT prostate lymphoscintigraphy is to use high-mA CT, commonly used for diagnostic multidetector CT scanners, instead of low-mA CT that is used in our studies, when combined with SPECT data. The high-mA CT can reveal higher details of small lymph nodes; thus the anatomical identification of lymph node locations from SPECT images will be easier.

CONCLUSION

We successfully performed a 10-patient study to establish a practice procedure of prostate lymphoscintigraphy using SPECT/CT with a general goal of translating tomographic lymph node identification information into radiation treatment planning. The use of filtered ^{99m}Tc -sulfur nanocolloid seems appropriate for this indication, and the 1.5–3 hour imaging time window is favorable in practice.

Acknowledgments

We thank Marilyn Robinson at UCSF for her help on the clinical study coordination. We also thank Chang-Lae Lee, who helped radiation dose calculations using biokinetic data. Y.S. was partially funded by National Cancer Institute Grant #K25 CA114254.

References

1. Spiotto MT, Hancock SL, King CR. Radiotherapy after prostatectomy: improved biochemical relapse-free survival with whole pelvic compared with prostate bed only for high-risk patients. *Int J Radiat Oncol Biol Phys.* 2007; 69:54–61. [PubMed: 17459606]
2. Weckermann D, Dorn R, Trefz M, Wagner T, Wawroschek F, Harzmann R. Sentinel lymph node dissection for prostate cancer: experience with more than 1,000 patients. *J Urol.* 2007; 177:916–920. [PubMed: 17296375]
3. Touijer K, Rabbani F, Otero JR, Secin FP, Eastham JA, Scardino PT, Guillonneau B. Standard versus limited pelvic lymph node dissection for prostate cancer in patients with a predicted probability of nodal metastasis greater than 1%. *J Urol.* 2007; 178:120–124. [PubMed: 17499306]
4. Briganti A, Karakiewicz PI, Chun FK, et al. Percentage of positive biopsy cores can improve the ability to predict lymph node invasion in patients undergoing radical prostatectomy and extended pelvic lymph node dissection. *Eur Urol.* 2007; 51:1573–1581. [PubMed: 17293026]
5. Briganti A, Gallina A, Suardi N, et al. A nomogram is more accurate than a regression tree in predicting lymph node invasion in prostate cancer. *BJU Int.* 2008; 101:556–560. [PubMed: 18005204]
6. Wagner M, Sokoloff M, Daneshmand S. The role of pelvic lymphadenectomy for prostate cancer--therapeutic? *J Urol.* 2008; 179:408–413. [PubMed: 18076938]
7. Roach M 3rd, DeSilvio M, Valicenti R, Grignon D, Asbell SO, Lawton C, Thomas CR Jr, Shipley WU. Whole-pelvis, "mini-pelvis," or prostate-only external beam radiotherapy after neoadjuvant and concurrent hormonal therapy in patients treated in the Radiation Therapy Oncology Group 9413 trial. *Int J Radiat Oncol Biol Phys.* 2006; 66:647–653. [PubMed: 17011443]
8. Ploysongsang SS, Aron BS, Shehata WM. Radiation therapy in prostate cancer: whole pelvis with prostate boost or small field to prostate? *Urology.* 1992; 40:18–26. [PubMed: 1621308]

9. Ganswindt U, Paulsen F, Corvin S, et al. Optimized coverage of high-risk adjuvant lymph node areas in prostate cancer using a sentinel node-based, intensity-modulated radiation therapy technique. *Int J Radiat Oncol Biol Phys.* 2007; 67:347–355. [PubMed: 17236960]
10. Warncke SH, Mattei A, Fuechsel FG, Z'Brun S, Krause T, Studer UE. Detection rate and operating time required for gamma probe-guided sentinel lymph node resection after injection of technetium-99m nanocolloid into the prostate with and without preoperative imaging. *Eur Urol.* 2007; 52:126–132. [PubMed: 17258385]
11. Alicikus ZA, Yamada Y, Zhang Z, Pei X, Hunt M, Kollmeier M, Cox B, Zelefsky MJ. Ten-year outcomes of high-dose, intensity-modulated radiotherapy for localized prostate cancer. *Cancer.* 2010 Nov 8. [Epub ahead of print].
12. Ganswindt U, Paulsen F, Corvin S, et al. Intensity modulated radiotherapy for high risk prostate cancer based on sentinel node SPECT imaging for target volume definition. *BMC Cancer.* 2005; 5:91. [PubMed: 16048656]
13. Jimenez IR, Roca M, Vega E, Garcia ML, Benitez A, Bajen M, Martin-Comin J. Particle sizes of colloids to be used in sentinel lymph node radiolocalization. *Nucl Med Commun.* 2008; 29:166–172. [PubMed: 18094639]
14. Holl G, Dorn R, Wengenmair H, Weckermann D, Sciuk J. Validation of sentinel lymph node dissection in prostate cancer: experience in more than 2,000 patients. *Eur J Nucl Med Mol Imaging.* 2009; 36:1377–1382. [PubMed: 19430782]
15. Vermeeren L, Muller SH, Meinhardt W, Valdes Olmos RA. Optimizing the colloid particle concentration for improved preoperative and intraoperative image-guided detection of sentinel nodes in prostate cancer. *Eur J Nucl Med Mol Imaging.* 2010; 37:1328–1334. [PubMed: 20306033]
16. Ganswindt U, Schilling D, Muller AC, Bares R, Bartenstein P, Belka C. Distribution of Prostate Sentinel Nodes: A SPECT-Derived Anatomic Atlas. *Int J Radiat Oncol Biol Phys.* 2010 Aug 28. [Epub ahead of print].
17. Alazraki NP, Eshima D, Eshima LA, Herda SC, Murray DR, Vansant JP, Taylor AT. Lymphoscintigraphy, the sentinel node concept, and the intraoperative gamma probe in melanoma, breast cancer, and other potential cancers. *Semin Nucl Med.* 1997; 27:55–67. [PubMed: 9122724]
18. Hung JC, Wiseman GA, Wahner HW, Mullan BP, Taggart TR, Dunn WL. Filtered technetium-99m-sulfur colloid evaluated for lymphoscintigraphy. *J Nucl Med.* 1995; 36:1895–1901. [PubMed: 7562061]
19. Stabin MG, Sparks RB, Crowe E. OLINDA/EXM: the second-generation personal computer software for internal dose assessment in nuclear medicine. *J Nucl Med.* 2005; 46:1023–1027. [PubMed: 15937315]
20. Wengenmair H, Kopp J, Vogt H, Wawroschek F, Grober S, Dorn R, Heidenreich P. Sentinel lymph node diagnosis in prostatic carcinoma: II. Biokinetics and dosimetry of 99mTc-Nanocolloid after intraprostatic injection. *Nuklearmedizin.* 2002; 41:102–107. [PubMed: 11989296]

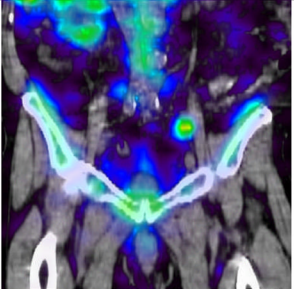
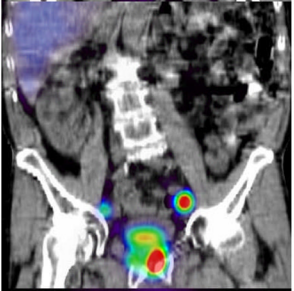
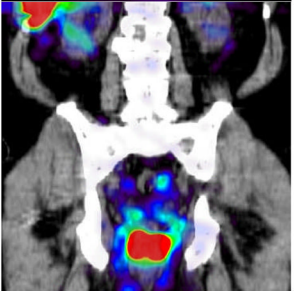
Patient	Age (y)	Injected dose (MBq)	Areas of lymph nodes identified	SPECT/CT
1	76	93	<ul style="list-style-type: none"> - Bilateral external iliac - Bilateral common iliac - Low aortocaval region 	
2	75	104	<ul style="list-style-type: none"> - Bilateral external iliac (left > right) - Bilateral common iliac - Bilateral paraaortic (up to the level of the renal arteries) 	
3	74	67	<ul style="list-style-type: none"> - Bilateral external iliac (left > right) - Bilateral common iliac - Bilateral low paraaortic - Left paraaortic up to the level of the renal artery 	

Figure 1. Age distribution, radiotracer administration, identified lymph node locations, and representative coronal view of SPECT/CT for the patients enrolled for this study (patients 1–3).

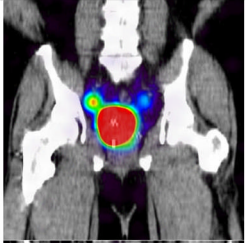
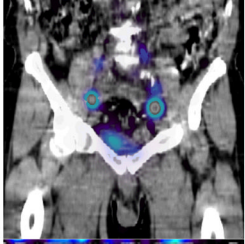
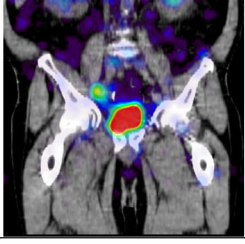
Patient	Age (y)	Injected dose (MBq)	Areas of lymph nodes identified	SPECT/CT
4	62	105	<ul style="list-style-type: none"> - Bilateral external iliac (right > left) - Bilateral common iliac - Bilateral paraaortic up to the level of the renal arteries 	
5	76	96	<ul style="list-style-type: none"> - Bilateral external iliac - Bilateral common iliac - Common iliac of the promontory - Subaortic common iliac - Bilateral paraaortic up to T12 level - Parapancreatic 	
6	78	41	<ul style="list-style-type: none"> - Bilateral external iliac - Bilateral internal iliac - Low bilateral paraaortic 	

Figure 2. Age distribution, radiotracer administration, identified lymph node locations, and representative coronal view of SPECT/CT for the patients enrolled for this study (patients 4–6)

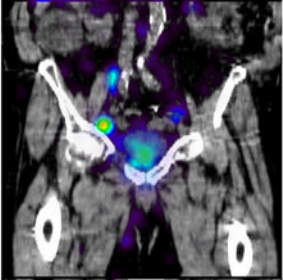
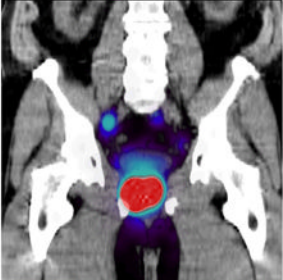
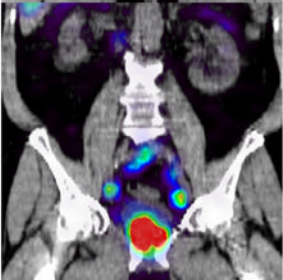
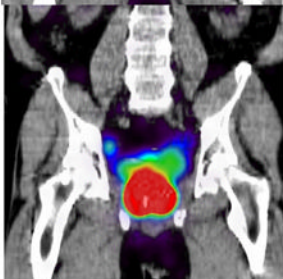
Patient	Age (y)	Injected dose (MBq)	Areas of lymph nodes identified	SPECT/CT
7	81	44	<ul style="list-style-type: none"> - Bilateral inguinal - Bilateral external iliac - Right common iliac 	
8	56	111	<ul style="list-style-type: none"> - Bilateral external iliac - Bilateral common iliac - Common iliac of the promontory - Subaortic common iliac 	
9	66	90	<ul style="list-style-type: none"> - Left inguinal - Bilateral external iliac - Bilateral common iliac - Common iliac of the promontory - Subaortic common iliac - Bilateral paraaortic lymph nodes up to T12 level 	
10	65	107	<ul style="list-style-type: none"> - Bilateral external iliac (right > left) - Bilateral common iliac (right > left) - Low left paraaortic 	

Figure 3. Age distribution, radiotracer administration, identified lymph node locations, and representative coronal view of SPECT/CT for the patients enrolled for this study (patients 7–10)

Table 1

Radiation dose estimates comparison between Nanocoll (reference data) and filtered ^{99m}Tc -sulfur nanocolloid (three patients).

Estimated absorbed dose (mSv/MBq)	Reference (Nanocoll) (20)	Patient 1	Patient 2	Patient 3
Whole Body (ED)	7.6	4.0	3.9	5.2
Bladder	11.3	12.8	13.8	21.1
Liver	26.3	10.6	10.9	8.1
Spleen	16.5	12.4	9.4	37.5
Marrow	22.1	5.8	4.2	4.0